FPGA implementation of a digital passband precoder for an all-digital underwater acoustic Massive MIMO transmitter

Jinfeng Li and Y. Rosa Zheng
{jili18,yrz218}@lehigh.edu
Dept. of Electrical and Computer Engineering, Lehigh University
Bethlehem, PA. 18015, U.S.A

ABSTRACT

This paper designs a digital passband precoder for an all-digital underwater acoustic massive MIMO transmitter. Taking the advantage of the low carrier frequency in the kilo-Hertz acoustic band, the proposed design utilizes Digital Up Converters (DUC), digital carrier modulators, digital amplitude controls, pulse width modulators, and digital phase shifters to implement the passband precoder in a hybrid beamforming (HBF) structure. In contrast to the existing RF analog precoder, the proposed design offers 8-bit amplitude and 10-bit phase-shift control, which provides a high degree of freedom in the precoder design. In addition, this design eliminates the digital to analog converters (DAC), analog local/RF oscillators, and analog modulators which are often the most power hungry devices. The proposed design is prototyped on a low-end FPGA XC7A100T. The results show that the maximum resource utilization is around 60% for an array size of 128 and different sub-array configurations yield similar low resource utilization and low power consumption. The design is also tested on a Nexys 4-based underwater acoustic transmitter with an array of 32 transducers.

KEYWORDS

Hybrid beamforming, digital passband precoder, all-digital underwater acoustic transmitter.

ACM Reference Format:
Jinfeng Li and Y. Rosa Zheng. 2022. FPGA implementation of a digital passband precoder for an all-digital underwater acoustic Massive MIMO transmitter. In *The 16th International Conference on Underwater Networks & Systems (WUWNet'22), November 14–16, 2022, Boston, MA, USA.* ACM, New York, NY, USA, 5 pages. https://doi.org/10.1145/3567600.3568153

1 INTRODUCTION

The Massive Multiple-Input-Multiple-Output (MIMO) technology [9] has been successfully adopted in the millimeter wave frequency bands for emerging 5G/6G terrestrial wireless communication systems, thanks to its channel hardening effect and huge gains in both spectrum efficiency and energy efficiency [10]. Practical massive MIMO schemes are often implemented by the hybrid beamforming (HBF) structure [10, 13, 14], as shown in Fig. 1, where the digital baseband (BB) precoder maps the data streams of U users into M sub-array groups. Denote m, i as the group index and sample index, respectively. The complex baseband digital signal $x_{m,i}$ is first converted into analog I and Q signals which are then modulated on to the intermediate frequency (IF) via a local oscillator. The IF chain outputs the analog modulated signal $r_{m,i}$ which is split into K RF branches of the passband analog precoders. Each analog RF precoder consists of an analog phase shifter (PS) and a variable gain amplifier (VGA) which compensates for amplitude distortion caused by the analog PS. The precoded signals are then transmitted by $N = MK$ antennas after the power amplifiers (PA).

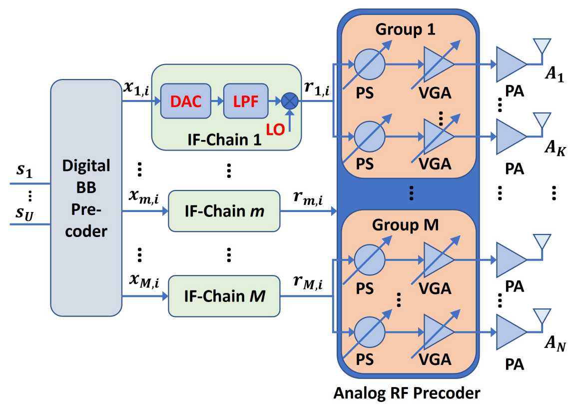

Figure 1: Sub-array architecture (SA) of hybrid beamforming (HBF) for RF massive MIMO base stations. DAC – digital to analog converter, LPF – Low-pass filter, LO – Local Oscillator, IF - Intermediate frequency, PS – phase shifter, VGA – Variable gain amplifier, PA – Power amplifier.

The potential of massive MIMO scheme is very much desired for underwater acoustic communication, because the severe multipath fading and the huge frequency-dependent signal attenuation of acoustic communication channels result in very limited usable frequency bands which are as low as 2 kHz - 200 kHz for medium and short communication ranges. The limited spectrum and energy resources have been the bottleneck even for point-to-point communications, let alone acoustic networks with multiple users. Therefore, utilizing massive MIMO for underwater acoustic communication and networking has attracted strong interest in recent years [1, 2, 5, 12, 15]. However, most of the work on the topic remains as theoretical analysis [12], computer simulations [1, 2], or receiver beamforming (instead of transmitter BF) [15]. The only hardware implementation is based on the digital baseband beamforming architecture [5] and it is unclear how the passband modulation and system integration were implemented.

WUWNet'22, November 14–16, 2022, Boston, MA, USA

ACM ISBN 978-1-4503-9952-4/22/11.
https://doi.org/10.1145/3567600.3568153

The hardware implementation of acoustic massive MIMO transmitter differs significantly from the RF precoder in several aspects. First, the RF system defaults that the baseband precoder is in digital form and the passband precoder is in analog form, because the IF and RF frequencies are in Mega-Hertz or Giga-Hertz ranges which is challenging to be implemented in digital forms. However, the performance of the analog beamforming is limited, especially in terms of fine tuning and null steering due to inaccurate control of analog PS and the lack of amplitude adjustment [11]. In contrast, underwater acoustic communication system uses low carrier frequencies on the order of kHz, thus having significant advantages to be implemented in full-digital form. Secondly, acoustic systems can implement carrier modulator via a digital up converter (DUC) and the modulated digital passband signals are usually converted into pulse-width modulation (PWM) signals which then drive the PAs and the acoustic transducers. As the acoustic transducer circuits are low-pass filter in nature, it also eliminates Digital to Analog Converters (DAC) often required by the IF chains. When the number of sub-array groups is large, eliminating the DAC, the intermediate frequency (IF) or carrier oscillator, and the analog modulator can result in significant energy and cost savings in a massive MIMO transmitter. Thirdly, fully digital passband precoding is easy to control in the PS and no VGA is required after the phase shifters.

This paper implements a digital passband precoder with the HBF structure for an all-digital underwater acoustic massive MIMO transmitter by varying the duty cycle and time delay of the passband PWM signals. The proposed design is prototyped on a low-end Xilinx Field Programmable Field Array (FPGA) platform XC7A100T which has up to 101K Logic Cells (LC), 240 DSP slices, and 4.86K memory banks (270×18 Kb BRAMs). The results show that the maximum resource utilization is around 60% for an array size of 128. Different sub-array configurations yield similar low resource requirement and low power consumption. An example of 32-element massive MIMO passband precoder is tested on the Nexys 4 Artix-7 FPGA Trainer Board hosting XC7A100T. The utilization of various resources is less than 15% of this low-end FPGA, making the design easy to expand to larger MIMO sizes. The capability of the amplitude adjustment and phase shift of the massive MIMO passband precoder is verified in a real-time underwater acoustic transmitter (UAT) with a carrier frequency of 115 kHz and a bandwidth of 34 kHz. The results show that different combinations of M and K in sub-array configurations result in similar resource usage and power consumption.

The main contributions of this paper are summarized as follows:

- A digital passband precoder in an HBF structure is proposed for underwater massive MIMO transmitter, which offers 8-bit amplitude and 10-bit phase-shift control. In contrast, the analog RF counterpart can achieve around 6-bit quantization for phase shifter and no amplitude adjustment. The proposed digital implementation provides a high degree of freedom for the precoder design.
- The proposed digital passband precoder separates the amplitude control and phase control to save hardware resources: amplitude control is employed before the PWM module, while the phase shift control is applied after the PWM module, thus reducing the consumption of LUT (Look Up Tables) and FF (Flip Flops).
- The proposed implementation on the FPGA platform has the advantage of flexible configuration with different array sizes and precoder designs. The resource utilization for an 128-element transmitter requires a small area and achieves low power consumption.

2 SYSTEM MODEL OF MASSIVE MIMO

Consider a massive MIMO single carrier modulation (SCM) communication system with HBF structure supporting U users, as shown in Fig. 2. The U data streams are processed by a digital baseband precoder and a passband precoder in the FPGA. The N precoded signals are sent out to the Front-end (FE) circuits to drive the class-D power amplifiers (PA) in the form of PWM signals. The goal of the massive MIMO transmitter is to allow different receivers to receive their own data streams with minimum interference among the U users.

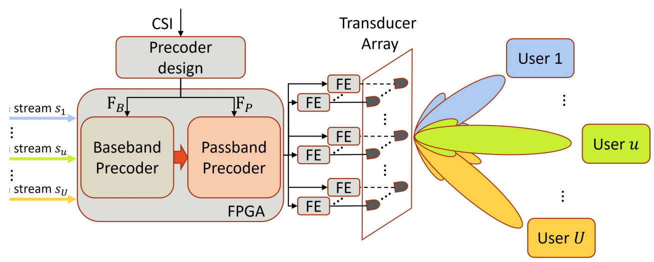

Figure 2: System Model of massive MIMO with N-transmiting antenneas and U-receiving users

In this work, we assume that linear precoding is designed for flat fading channels. In the case of frequency selective channels, precoding can be extended to per sub-carrier precoding using Frequency Division Multiple Access (FDMA). Assume the channel matrix $\mathbf{H}$ is known from the estimated CSI. The baseband digital precoder matrix $\mathbf{F}_B$ and passband digital precoder $\mathbf{F}_P$ is obtained, normally by a two-stage design [4, 14]. Therefore, the received symbol $\mathbf{y}_u$ at the uth user in the baseband equivalent model is denoted as

$$\mathbf{y}_u = \sqrt{\rho}\mathbf{H}\mathbf{F}_P\mathbf{F}_B\mathbf{s} + \mathbf{w} \tag{1}$$

where $\mathbf{s} \in C^{U\times 1}$ is the transmitted symbols of all users, $\mathbf{F}_B \in C^{M\times U}$, $\mathbf{F}_P \in C^{N\times M}$, $\mathbf{H} \in C^{N_r\times N}$, N_r is the number of transducers equipped on the user, ρ is the average received power, and $\mathbf{w}$ is the noise vector. The precoder $\mathbf{F}_P$ and $\mathbf{F}_B$ needs to meet the total transmit power constraint: $\| \mathbf{F}_P\mathbf{F}_B \|_{\mathbf{F}} \leq U$. Different from the analog precoder in RF systems, the proposed digital precoder for underwater massive MIMO has no amplitude constraints on the passband precoder $\mathbf{F}_P$, whose matrix form is depicted in (2), where $\mathbf{p}_i = [p_{(i-1)K+1,i}, p_{(i-1)K+2,i}, \cdots, p_{iK,i}]^T, i = 1\cdots M$. The element $p_{k,m} = v_{m,k}\underline{/\phi_{m,k}}$, where $v_{m,k}$ and $\phi_{m,k}$ are the amplitude and the phase for the k_{th} branch in the m_{th} group, respectively. This all digital implementation of underwater massive MIMO precoder alleviates the difficulties experienced in the RF precoder design [10] due to strong constraints in analog precoder implementations.

$$\mathbf{F}_P = \begin{bmatrix} \mathbf{p}_1 & 0 & \cdots & \cdots & 0 \\ 0 & \mathbf{p}_2 & 0 & \cdots & \vdots \\ \vdots & 0 & \ddots & \cdots & \vdots \\ \vdots & \vdots & \cdots & \mathbf{p}_{M-1} & 0 \\ 0 & \cdots & \cdots & 0 & \mathbf{p}_M \end{bmatrix} \quad (2)$$

3 THE PROPOSED DIGITAL PASSBAND PRECODER

The proposed digital passband precoder in the HBF structure is shown in Fig. 3, where the data streams of U users are first processed by the digital baseband precoder which functions similar to the RF massive MIMO counterpart in Fig. 1. The mapped M baseband signals are digitally modulated by the M DUCs, respectively. Each DUC output is then split into K passband precoder branches consisting of an amplitude control (AC) module, a PWM module, and a digital PS. The resulting passband signals in terms of groups of pulse train are transmitted through N PAs and transducers. It is worth noting that the VGAs required by analog precoders are removed in the digital passband precoders as the digital phase shifters, unlike the analog phase shifters, would keep the amplitude of the passband signals unchanged so no VGA compensation is needed.

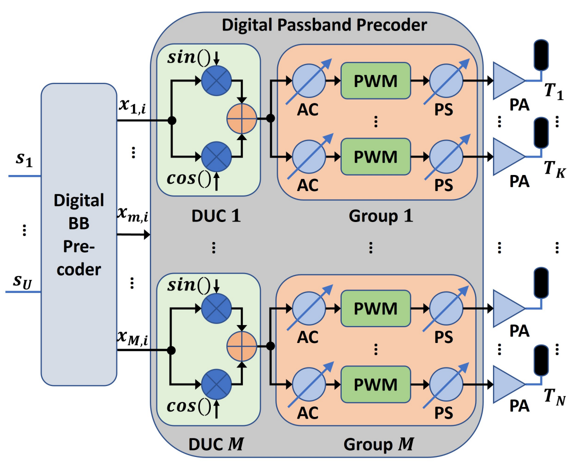

Figure 3: The proposed all-digital baseband and passband precoders in the HBF structure.

In the DUC module, the baseband samples are interpolated at a ratio of r_s and then converted to the passband samples by multiplying the digital carrier. To simplify the implementation, this paper selects $r_s = 4$ so that every carrier frequency is $f_c = f_s/r_s$ and both the cos and sin components of the carrier are represented simply by four values $\{0, 1, 0, -1\}$. Therefore, no multiplier is required for the digital carrier modulator.

Utilizing PWM for signal generation was also found in [3, 8] for RF MIMO systems. The proposed precoder differs from the implementation in [3, 8] is that the AC module is placed after the DUC module to adjust the amplitude of the passband signal (or the duty cycle of the PWM) while the structure in [3, 8] places a delta-sigma modulator (DSM) before the DUC module to represent a baseband signal. Besides, the proposed precoder implements the phase shift by an 1-bit width block Random Access Memory (RAM) and a timer for delaying the output of the PWM signal. This approach reduces the amount of RAM resource needed in the phase shift.

The implementation details of the passband precoder are shown in Fig. 4, where m, k, i are the group, branch, and sample indexes, respectively. Please note that the amplitude and phase shift are separately controlled before the PWM module and after the PWM module.

Denote $r_{m,k,i}$ as the samples of passband waveform duplicated from the output of the m_{th} DUC module, $v_{m,k}$ as the amplitude weight for the k_{th} branch in the m_{th} group. Therefore, $d_{m,k,i}$ is the amplitude-weighted passband samples and $-Q/2 \leq d_{m,k,i} \leq Q/2$ with Q being the peak-to-peak amplitude of the precoded signal. Adding $Q/2$ to $d_{m,k,i}$ yields the level-shifted signal $w_{m,k,i}$ which is the input to the PWM module. The binary pulse train at the output of the PWM module for all the passband samples are then stored into a 1-bit wide block Random Access Memory (RAM). The phase shift is realized by reading out all the binary pulse trains from the block RAM at different time delay $t_{m,k}$.

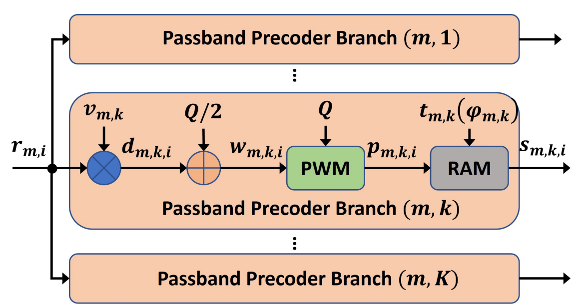

Figure 4: The data processing in one passband chain of the proposed digital passband precoder, where m, k, i are the group index, branch index, and data sample index, respectively.

To represent a passband sample with a binary pulse train, the PWM module needs to work at a frequency of f_{pwm} which is much higher than the sampling frequency f_s of the passband signals. The maximum amplitude that can be represented by the PWM module is

$$Q = f_{pwm}/f_s \quad (3)$$

Therefore, the resolution of the amplitude control AC_r is limited by

$$AC_r = \frac{1}{Q} = \frac{1}{\frac{f_{pwm}}{f_s}} = \frac{r_s f_c}{f_{pwm}} \quad (4)$$

Several PWM implementations are discussed in [8]. In this work, we adopted the intuitive and simple PWM implementation method, where a comparator takes the input passband samples $w_{m,k,i}$ and compares it to a saw-tooth signal with a period of $1/f_s$ and an amplitude increment from 0 to $Q - 1$. The comparator and the PWM output $p_{m,k,i}$ are illustrated in Fig. 5. In every PWM period, a counter starts from 0 and accumulates to the full range Q to yield the saw-tooth. The output is initially set to one and is toggled to zero at the trigger of the comparator output. At the end of the PWM period, the output is set to 1 again ready for the next sample of the passband signal.

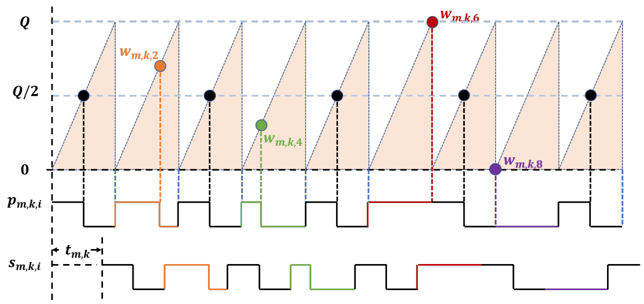

Figure 5: The waveforms generated by the PWM and the phase shifter.

Since the baseband signal has been modulated to the passband signal after the DUC module, the amplitude weights needed in the AC module are real numbers. Therefore, for one branch, only one multiplier is required. The total number of multipliers needed in a massive array system increases linearly with the total number of branches in the digital passband precoder.

It is feasible to realize the phase shift on the 1-bit PWM waveform in FPGA. In this work, we use one 18k block RAM for each branch that supports a large delay up to $16384/f_{pwm}$ second. The resolution for the phase shift ϕ_r on the carrier frequency f_c can be obtained by

$$\phi_r = \frac{2\pi}{Q \cdot r_s} = \frac{2\pi}{\frac{f_{pwm}}{f_s} \cdot \frac{f_s}{f_c}} = \frac{2\pi f_c}{f_{pwm}} \tag{5}$$

4 SYNTHESIS AND PERFORMANCE RESULTS

The proposed digital passband precoder was implemented on the Nexys 4 trainer board which has an Artix-7 FPGA (XC7A100T-1CSG324C, 63,400 LUTs, 126,800 FFs, 270 18Kb BRAMs, 240 DSP48Es). The parameters used in the design are

- Array size $N = MK = 32, 64,$ and 128;
- transmitter carrier frequency $f_c = 115$ kHz, DUC sampling rate $f_s = 4f_c$;
- PWM clock frequency $f_{pwm} = 184$ MHz, max amplitude $Q = 400$. Amplitude weight format Q1.7.

The implemented digital passband precoder was tested on a test platform which includes a host PC, an all-digital underwater acoustic transmitter (UAT) based on Nexys 4 FPGA board, Class-D Power Amplifiers (PA), frequency Matching Circuit (MC), and omnidirectional acoustic transducers [7]. The platform is shown in Fig. 6, where only four channels are shown for good resolution.

A GUI running on the host PC loaded the information bits and the configuration parameters through an USB to UART cable. The UAT consists of a rate-1/2 non-systematic convolutional encoder, a 32×32 block ping-pong interleaver, a bit to symbol mapper (M-phase-shift keying), a pulse shaping filter, and a digital passband precoder. The digital baseband precoder was a simple $1 \times M$ unitary vector converting the one data stream to M sub-array groups. The resource utilization after place-and-route of the all-digital UAT for different array sizes $N = MK = 32, 64,$ and 128 is listed in Table 1.

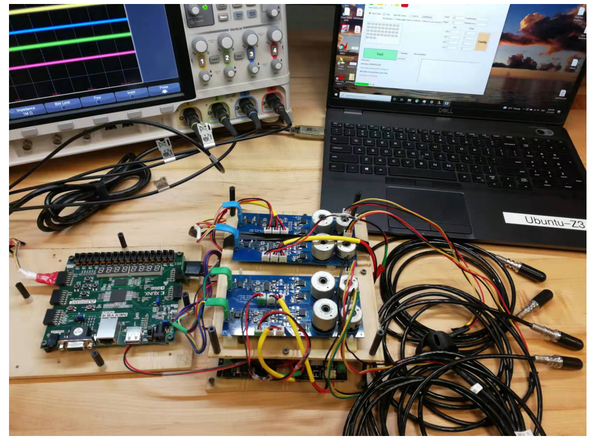

Figure 6: The test platform for the proposed digital passband precoder.

Table 1: Resource utilization FOR DIFFERENT ARRAY SIZE N=32, 64, and 128

Resource	M=2, K=16	M=4, K=16	M=8, K=16
BRAM (18k)	102 (37%)	135 (48%)	203 (72%)
DSP48E	34 (14%)	68 (30%)	136 (60%)
LUT	5652 (7%)	10126 (19%)	19022 (35%)
FF	5289 (4%)	9186 (8%)	16857 (15%)
Max. Freq. (MHz)	218.19	217.94	217.94
Power consumption	0.335 W	0.535 W	0.970 W

It is notable that 30% of the block BRAM was used by the baseband signal processing as a large buffer was instantiated in this design to support different modulation schemes, such as Frequency-Hopped (FH) Binary Frequency Shift Keying (BFSK). Therefore, for example, the passband precoder only used 7% of the BRAM for the array size $N = 32$. From Table 1, the achieved maximum frequency of the design is about 218 MHz which is much higher than the clock frequency of 184 MHz needed in the design. The maximum resource utilization is the DSP48E, but it is still only about 60% of this low-end FPGA for the array size of 128.

Besides,The detailed resource utilization for different sub-array configurations of the array size $N = 32$ was listed in Table 2. With different M, K configurations, the resource utilization and power consumption are similar as long as $N = MK$ remains the same.

An oscilloscope DSOX1204G was used to capture the PWM outputs from the all-digital UAT. Fig. 7 depicts the first four branches in the first group. The amplitude adjustment on the passband samples is shown in Fig. 7(a). The four waveforms from top to bottom represents the PWM outputs of the first four branches with the amplitude weights $v_{1,1} = 1$, $v_{1,2} = 0.75$, $v_{1,3} = 0.5$, and $v_{1,2} = 0.25$, respectively. All branches had the same phase shift. Fig. 7(b) shows the Phase shift of the first four channels with the same amplitude weight of 1,

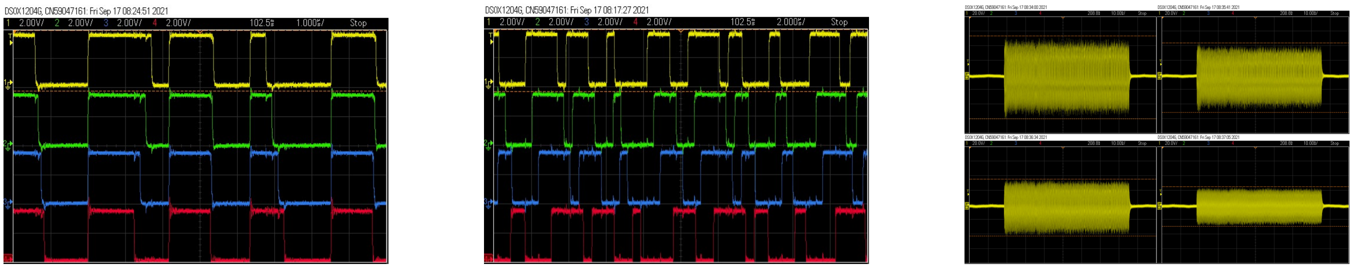

(a) (b) (c)

Figure 7: PWM outputs for the first 4 branches in the first group. (a) The weighted amplitudes. (b) phase-shifts. (c) The transmit signals at one branch adjusted by different amplitude weights $v_{m,k}$ in the AC

Table 2: Resource utilization of the UAT when f_c=115 kHz and $N = 32$

Resource	M=1, K=32	M=2, K=16	M=4, K=8
BRAM (18k)	100 (37%)	102 (37%)	104 (39%)
DSP48E	33 (13%)	34 (14%)	36 (15%)
LUT	5750 (9%)	5652 (7%)	5847 (9%)
FF	5293 (4%)	5289 (4%)	5563 (4%)
Max. Freq. (MHz)	217.03	218.19	218.78
Power consumption	0.347 W	0.335 W	0.340 W

where the phase delays were set to $t_{1,1} = 0$, $t_{1,2} = 22.5°$, $t_{1,3} = 45°$, and $t_{1,4} = 90°$. The phase shifts were accurately achieved on the hardware test points. Also the PWM amplitudes were maintained without distortion.

In addition, the modulated transmit signals were tested with the oscilloscope on the acoustic transducers, as shown in Fig. 7(c), where the modulated signals of one branch exhibited different amplitudes corresponding to the different amplitude weights set in Fig. 7(a). To eliminate the effect caused by the amplification gain difference among PAs, comparisons among different transducers are omitted here. In practice, the difference in PA gains may be eliminated by fine tuning the PA hardware or compensated through the passband precoder.

5 CONCLUSION

This paper has proposed and implemented a digital passband precoder for an all-digital acoustic underwater massive MIMO transmitter. Benefiting from the kHz carrier frequency band of acoustic communications, the proposed design utilizes the DUC for digital passband carrier modulation and uses the PWM to represent the passband signal digitally. Thus, the proposed digital passband precoder offers both the amplitude and phase shift control. The low-pass filter nature of acoustic transducers also helps to eliminate the power-hungry DACs commonly required in RF passband precoders. The proposed digital passband precoder has been prototyped on a Xilinx Nexys 4 Artix-7 FPGA trainer board. With an array size of 128 transducers, the implementation utilizes 60% of the resources of this low-end platform. Future work will include performance analysis in terms of spectral efficiency, precoder design according to the channel conditions or simplified beam switching [6], and experimental evaluation in the field.

REFERENCES

[1] Mohammud J Bocus, Dimitris Agrafiotis, and Angela Doufexi. 2018. Real-time video transmission using massive MIMO in an underwater acoustic channel. In *2018 IEEE Wireless Communications and Networking Conference (WCNC)*. IEEE, 1–6.

[2] Mohammud J Bocus, Angela Doufexi, and Dimitris Agrafiotis. 2018. MU-massive MIMO for UWA communication. In *2018 IEEE 88th Vehicular Technology Conference (VTC-Fall)*. IEEE, 1–5.

[3] Rui Fiel Cordeiro, Arnaldo SR Oliveira, and José MN Vieira. 2015. All-digital transmitter with a mixed-domain combination filter. *IEEE Trans. Circuits and Systems II: Express Briefs* 63, 1 (2015), 4–8.

[4] Omar El Ayach, Sridhar Rajagopal, Shadi Abu-Surra, Zhouyue Pi, and Robert W Heath. 2014. Spatially sparse precoding in millimeter wave MIMO systems. *IEEE transactions on wireless communications* 13, 3 (2014), 1499–1513.

[5] Bello Lawal, Syed Saad Azhar Ali, and Azlan Bin Awang. 2016. Massive MIMO systems for underwater acoustic communication. In *2016 IEEE International Conference on Underwater System Technology: Theory and Applications (USYS)*. IEEE, 159–164.

[6] Byung Moo Lee. 2020. Adaptive Switching Scheme for RS Overhead Reduction in Massive MIMO With Industrial Internet of Things. *IEEE Internet of Things Journal* 8, 4 (2020), 2585–2602.

[7] Jinfeng Li, Joseph Hall, and Y Rosa Zheng. 2020. Utilizing JANUS for Very High Frequency Underwater Acoustic Modem. In *Global Oceans 2020: Singapore–US Gulf Coast*. IEEE, 1–6.

[8] Daniel Markert, Xin Yu, Holger Heimpel, and Georg Fischer. 2016. An all-digital, single-bit RF transmitter for massive MIMO. *IEEE Trans. Circuits and Systems I: Regular Papers* 64, 3 (2016), 696–704.

[9] Thomas L. Marzetta. 2015. Massive MIMO: An Introduction. *Bell Labs Technical Journal* 20 (2015), 11–22. https://doi.org/10.15325/BLTJ.2015.2407793

[10] Andreas F Molisch, Vishnu V Ratnam, Shengqian Han, Zheda Li, Sinh Le Hong Nguyen, Linsheng Li, and Katsuyuki Haneda. 2017. Hybrid beamforming for massive MIMO: A survey. *IEEE Communications Magazine* 55, 9 (2017), 134–141.

[11] Ada SY Poon and Mazhareddin Taghivand. 2012. Supporting and enabling circuits for antenna arrays in wireless communications. *Proc. IEEE* 100, 7 (2012), 2207–2218.

[12] Wenqian Wu, Xiqi Gao, Chen Sun, and Geoffrey Ye Li. 2021. Shallow Underwater Acoustic Massive MIMO Communications. *IEEE Trans. Signal Processing* 69 (2021), 1124–1139. https://doi.org/10.1109/TSP.2021.3050037

[13] Han Yan, Sridhar Ramesh, Timothy Gallagher, Curtis Ling, and Danijela Cabric. 2019. Performance, power, and area design trade-offs in millimeter-wave transmitter beamforming architectures. *IEEE Circuits and Systems Magazine* 19, 2 (2019), 33–58.

[14] Didi Zhang, Yafeng Wang, Xuehua Li, and Wei Xiang. 2017. Hybridly connected structure for hybrid beamforming in mmWave massive MIMO systems. *IEEE Trans. Communications* 66, 2 (2017), 662–674.

[15] Xueyuan Zhao and Dario Pompili. 2015. AMMCA: Acoustic massive MIMO with carrier aggregation to boost the underwater communication data rate. In *Proceedings of the 10th International Conference on Underwater Networks & Systems*. 1–5.